Current-Induced Stabilization of Surface Morphology in Stressed Solids

Vivek Tomar, M. Rauf Gungor, and Dimitrios Maroudas*

Department of Chemical Engineering, University of Massachusetts, Amherst, Massachusetts 01003-3110, USA

(Received 20 July 2007; published 24 January 2008)

We examine the surface morphological evolution of a conducting crystalline solid under the simultaneous action of an electric field and mechanical stress based on a fully nonlinear model and combining linear stability theory with self-consistent dynamical simulations. We demonstrate that electric current, through surface electromigration, can stabilize the surface morphology of the stressed solid against cracklike surface instabilities. The results also have more general implications for the morphological response of solid surfaces under the simultaneous action of multiple external forces.

DOI: 10.1103/PhysRevLett.100.036106 PACS numbers: 68.35.Ja, 05.70.Ln, 62.20.Mk, 66.30.Qa

Surface morphological stability underlies a broad class of materials processing, function, and reliability problems in numerous technological applications. Commonly, stability and pattern formation are studied in response to the action of an external force on the material system of interest, while the effects of simultaneous action of multiple external forces are studied less commonly or systematically. Nevertheless, the combined action of external fields has been known to affect significantly pattern formation in various complex systems. For example, light affects the electric-field induced assembly of micrometer-sized colloidal particles leading to optically tunable micropatterns [1]. As another example, a uniform magnetic field directed perpendicularly to the horizontal interface between a magnetizable and a nonmagnetic fluid with the denser fluid located below the interface can destabilize the flat fluid-fluid interface and induce the formation of interfacial patterns [2]. Here, we focus on the surface morphological stability of electrically conducting crystalline solids, metals or semiconductors, under stress, which are particularly important in applications ranging from aerospace and nuclear engineering to microelectronics and nanofabrication. Various stress-induced catastrophic defects, ranging from dislocations to cracks, in the component or device may be prevented through stabilization of the surface morphology by the action of external forces. However, to date, for surfaces of solids under the simultaneous action of multiple external fields, little is known about stabilizing effects, stability domain boundaries, morphological transitions to increasingly complex stable states, as well as instability mechanisms.

Linear stability analyses for the surface morphology of stressed elastic solids have predicted that the competition between elastic strain energy and surface energy can cause the growth of shape perturbations and specified the conditions (stress level, surface tension, perturbation wavelength) for the onset of morphological instability [3–5]; this is the well known Asaro-Tiller or Grinfeld (ATG) instability. In addition, numerical simulations accounting for important nonlinearities have addressed the surface dynamics beyond the instability onset and revealed instability mechanisms. For example, it has been demonstrated that a planar surface of a stressed elastic solid can evolve rapidly into a cusped surface, with smooth tops and deep cracklike grooves by surface diffusion [6], in agreement with experimental observations [7]. Moreover, dynamical simulations of electromigration (EM)-driven void morphological evolution in stressed metallic thin films demonstrated the formation of cracklike features emanating from void surfaces [8–10], including propagating faceted slits [9,10], due to an ATG instability. Recent theoretical work also addressed problems of EM-induced surface morphological evolution and stability of unstressed conductors and predicted the formation of various interesting surface features, including surface wave patterns [11,12], and complex oscillatory response of single-layer islands on crystalline substrates [13]. However, the surface morphological stability of a stressed crystalline conductor under the simultaneous action of an electric field remains elusive.

The purpose of this Letter is to analyze the surface morphological response of a conducting crystalline solid under the simultaneous action of an electric field and mechanical stress. We examine the possibility of current-induced stabilization of the surface morphology, driven by surface EM, in electrically conducting stressed solids that would otherwise undergo cracklike surface (ATG) instabilities. Using linear stability theory (LST) in conjunction with self-consistent dynamical simulations according to a fully nonlinear model of surface morphological evolution, we demonstrate that such surface stabilization is possible and specify the stability domain boundaries under certain conditions.

In our analysis, we examine the morphological stability of a planar surface following a continuum model of surface mass transport. We consider a semi-infinite, single-crystalline, electrically conducting solid body with a traction-free surface perturbed about the planar morphology under a uniform uniaxial stress of magnitude σ_∞ and an electric field of magnitude E_∞ that are both directed along x in a Cartesian frame of reference. The surface flux

of atoms, $\mathbf{J}_s = J_s\hat{\mathbf{s}}$, is expressed as

$$J_s = \frac{D_s\delta_s}{\Omega k_B T}\left\{-E_s q_s^* + \frac{\partial\mu}{\partial s}\right\}, \tag{1}$$

where D_s is the surface atomic diffusivity, δ_s/Ω is the number of surface atoms per unit area, Ω is the atomic volume, k_B is Boltzmann's constant, T is temperature, E_s is the electric-field component tangent to the surface, q_s^* is an effective surface charge, μ is the chemical potential of an atom on the surface, and s is the arc length along the surface with $\hat{\mathbf{s}}$ being the corresponding unit vector in a 2D representation assuming no morphological variations along z. We account for surface diffusional anisotropy through an anisotropy function, $f(\theta) \geq 1$ with $\theta \equiv \tan^{-1}(dy/dx)$, and write $D_s(\theta) = D_{s,\min} f(\theta)$, where $D_{s,\min}$ is the minimum surface diffusivity corresponding to a specific surface orientation. Isotropic linear elasticity yields

$$\mu(x) = \mu_0 - \gamma\Omega\kappa(x) + \frac{\Omega}{2M}\sigma_{\tau\tau}^2(x). \tag{2}$$

In Eq. (2), μ_0 is the chemical potential for a flat unstressed surface, γ is the isotropic [10] surface free energy per unit area, M is the elastic modulus, $\sigma_{\tau\tau}$ is the stress component tangential to the surface, and κ is the local surface curvature: parameterizing the surface morphology with the height function $y = h(x, t)$ gives $\kappa = (d^2h/dx^2) \times [1 + (dh/dx)^2]^{-3/2}$. Mass conservation yields

$$\frac{\partial h}{\partial t} = -\Omega\frac{\partial J_s}{\partial x}. \tag{3}$$

We start with a low-amplitude sinusoidal perturbation from the planar surface morphology, $h(x, 0) = \Delta_0 \sin kx$ with $\Delta_0 k \ll 1$, and examine the surface profile evolution $h(x, t)$. In our LST, we employ the local approximation $E_s = E_\infty \cos\theta$ [14] and the leading-order analytical solution $\sigma_{\tau\tau}^2 = \sigma_\infty^2 + 4\Delta_0 k\sigma_\infty^2 \sin(kx)$ [5]. Combining the above expressions with Eqs. (1)–(3), introducing the diffusional time scale $\tau \equiv k_B T l^4/(D_{s,\min}\delta_s\gamma\Omega)$ with a length scale l and the dimensionless variables $\tilde{h} \equiv h/l$, $\tilde{x} \equiv x/l$, and $\tilde{t} \equiv t/\tau$, and linearizing Eq. (3) within the small-slope approximation ($\partial\tilde{h}/\partial\tilde{x} \ll 1$) yields the dimensionless linearized evolution equation

$$\frac{\partial\tilde{h}}{\partial\tilde{t}} = \frac{E_\infty q_s^* l^2}{\gamma\Omega}\left(\frac{df}{d\theta}\bigg|_{\theta=0}\right)\frac{\partial^2\tilde{h}}{\partial\tilde{x}^2} - f(\theta=0)\frac{\partial^4\tilde{h}}{\partial\tilde{x}^4} - \frac{\sigma_\infty^2 l}{\gamma M}\frac{f(\theta=0)}{2}\frac{\partial^2}{\partial\tilde{x}^2}[4\Delta_0 k\sin(\tilde{k}\tilde{x})]. \tag{4}$$

Substituting $\tilde{h}(\tilde{x}, \tilde{t}) = \tilde{h}(\tilde{x}, 0)e^{\omega\tilde{t}}$ into Eq. (4) and setting $l \equiv \gamma M/\sigma_\infty^2$ [5,6] yields the dimensionless dispersion relation

$$\omega(\tilde{k}) = -\left(\frac{df}{d\theta}\bigg|_{\theta=0}\right)\Xi\tilde{k}^2 + 2f(\theta=0)\tilde{k}^3 - f(\theta=0)\tilde{k}^4. \tag{5}$$

In Eq. (5), $\omega(\tilde{k})$ is the rate of growth or decay of the perturbation from the planar surface morphology, $\tilde{k} \equiv kl$, $\theta = 0$ corresponds to the planar morphology, and

$$\Xi \equiv \frac{E_\infty q_s^*}{\gamma\Omega}\left(\frac{\gamma M}{\sigma_\infty^2}\right)^2 \tag{6}$$

expresses the relative strength of the two externally applied forces, electric field (E_∞) and stress (σ_∞), scaled with the capillary force.

Representative LST results are plotted in Fig. 1 for the functional form $f(\theta) = 1 + A\cos^2[m(\theta + \phi)]$ for a face-centered cubic metal such as Al or Cu; the dimensionless parameters A, m (an integer parameter), and ϕ determine the strength of the anisotropy, symmetry due to surface crystallographic orientation, and misorientation of a fast surface diffusion direction with respect to the applied electric-field direction, respectively. This anisotropy function has given results in excellent qualitative agreement with experiments of void morphological evolution in metallic thin films under EM conditions [10,15]. The results of Fig. 1 are for $A = 10$, $m = 3$ (corresponding to a $\langle 111\rangle$-oriented surface), and $\phi = -15°$. At $\Xi = 0$, there is no electric-field action and the planar surface undergoes an ATG instability for perturbations with $\tilde{k} < \tilde{k}_c$, i.e., for long wavelengths, $\lambda > \lambda_c$. Under such conditions, the $\omega(\tilde{k})$ curve exhibits a single maximally unstable wavelength for which the characteristic frequency, $\omega > 0$, attains its maximum value leading to rapid growth of the perturbation. As Ξ increases, i.e., as E_∞ increases at given σ_∞, the LST predicts that (i) the band of unstable wavelengths is narrowed, i.e., the surface is stabilized against some shorter-λ range that would trigger an unstable response at $\Xi = 0$, (ii) at higher Ξ, the $\omega(\tilde{k})$ curve may exhibit two maxima (see Fig. 1 for $\Xi = 0.16$), including one at $\tilde{k} = 0$ with $\omega(0) = 0$, which narrows even further the band of unstable

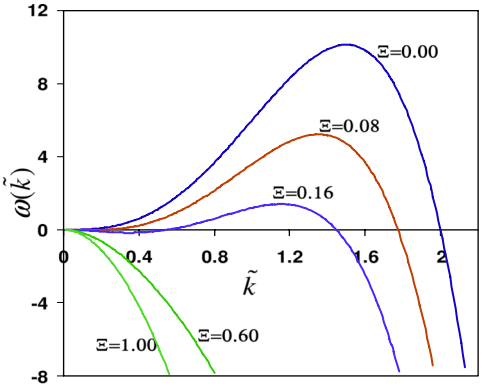

FIG. 1 (color online). Dispersion relations for various Ξ values giving the dependence of the characteristic dimensionless frequency, ω, for the growth ($\omega > 0$) or decay ($\omega < 0$) rate of a shape perturbation from a planar surface morphology on the dimensionless wave number, $\tilde{k}$, of the perturbation for surface diffusional anisotropy parameters $A = 10$, $m = 3$, and $\phi = -15°$.

wavelengths, and (iii) at Ξ higher than a certain critical value, Ξ_c, the range of unstable wave numbers vanishes and the planar surface is stabilized against any wavelength of shape perturbation. Setting $\omega = 0$ for $\tilde{k} > 0$ in Eq. (5) and demanding a double root for the resulting quadratic equation yields $\Xi_c = f(\theta)/(df/d\theta) = 0.20$ for the anisotropy parameters of Fig. 1. Consequently, application of a sufficiently strong electric field stabilizes fully the surface morphological response. This finding implies that electric current can stabilize surfaces of stressed solids that are otherwise vulnerable to cracking through an ATG instability.

To verify the main implications of the LST, we carried out dynamical simulations according to the fully nonlinear model of surface morphological evolution, Eqs. (1)–(3). In the simulations, the electrostatic potential Φ and elastic displacement $\mathbf{u}$ fields are computed through a Galerkin boundary-integral method [16] coupled self consistently with the evolving surface morphology expressed in a local coordinate system $(\hat{\mathbf{s}}, \hat{\mathbf{n}})$ and using an adaptive mesh; the surface propagation is monitored by time stepping $\partial u_n/\partial t = -\Omega \partial J_s/\partial s$, i.e., Eq. (3) expressed in the local surface coordinates, according to the interface tracking method of Refs. [10,15]. In this notation, $\hat{\mathbf{n}} \cdot \hat{\mathbf{s}} = 0$ and u_n is the local surface displacement normal to the surface. The mathematical formulation of the boundary-value problems for Φ and $\mathbf{u}$ has been presented in detail in Ref. [10] and can be easily adapted to the present computational domain. At a given set of parameters (Ξ, A, m, ϕ, k), $\tilde{h}(\tilde{x}, \tilde{t})$ is monitored for $\tilde{h}(\tilde{x}, 0) = \tilde{\Delta}_0 \sin(\tilde{k}\tilde{x})$ with $\tilde{\Delta}_0 \tilde{k} \ll 1$. A systematic exploration of parameter space has been conducted and representative (fully convergent) results are shown in Fig. 2.

Figure 2(a) shows the surface morphological response at $\Xi = 0$. An ATG instability triggers the formation of cusp-like surface features, which evolve to cracked grooves that propagate into the elastic solid. The lack of symmetry in the surface morphologies of Fig. 2(a) with respect to the crack plane is due to the surface diffusional anisotropy in our model. Under a weak electric field, $\Xi < \Xi_c$, the surface morphological response resembles that of Fig. 2(a) because the applied electric field is not strong enough to inhibit the ATG instability.

Under the action of a strong electric field, however, the ATG instability is indeed inhibited and surface cracking is prevented. This is shown clearly in Fig. 2(b), at $\Xi = 0.60 > \Xi_c$, which demonstrates that the initial sinusoidal disturbance decays back to the original planar morphology. The observed drift from right to left is due to surface EM. Figure 2(c) shows the surface morphological evolution in a case where a strong electric field, $\Xi = 0.60$, is turned on, then it is turned off for some time, and then it is turned back on. When the electric field is on, the initial disturbance decays, but when the field is turned off, the morphological instability is triggered and deep surface grooves develop. This response toward surface cracking is "healed" when

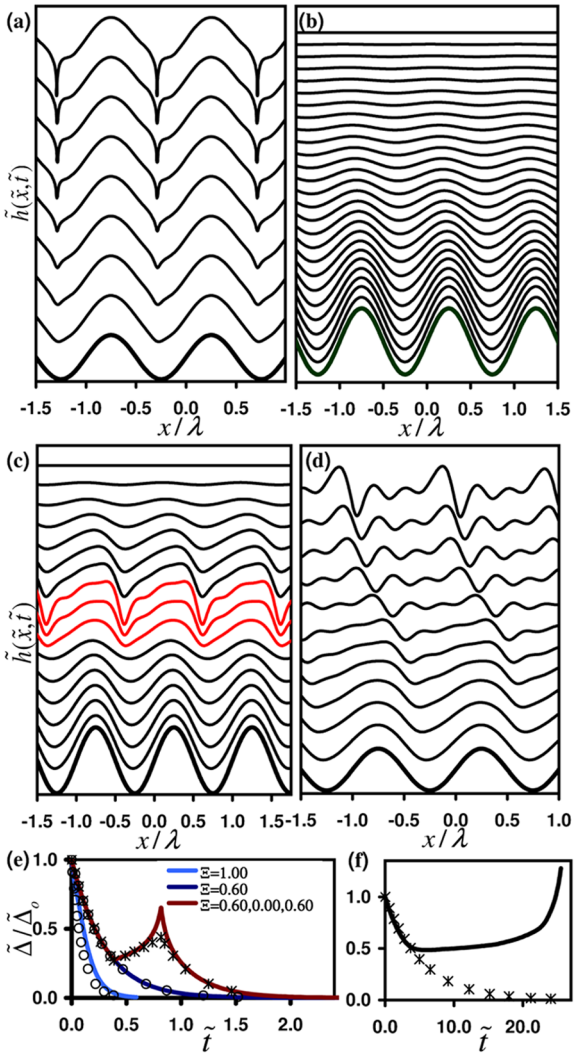

FIG. 2 (color online). Surface morphological evolution, $\tilde{h}(\tilde{x}, \tilde{t})$, starting with a perturbation $\tilde{h}(\tilde{x}, 0) = \tilde{\Delta}_0 \sin(\tilde{k}\tilde{x})$, at (a) $\Xi = 0.0$ for $\tilde{k} = 0.8$ and $\tilde{\Delta}_0/\tilde{\lambda} = 0.05$, where $\tilde{\lambda} \equiv \lambda/l$; (b) $\Xi = 0.60$ for $\tilde{k} = 0.50$ and $\tilde{\Delta}_0/\tilde{\lambda} = 0.02$; (c) same shape perturbation and Ξ value as in (b) but the electric current is turned off from $t = 0.38$ to $t = 0.81\tau$ and then it is turned back on; and (d) $\Xi = 0.16$ for $\tilde{k} = 0.35$ and $\tilde{\Delta}_0/\tilde{\lambda} = 0.005$. The anisotropy parameters are the same with those that yielded the dispersion curves of Fig. 1. The evolution sequences are from the bottom to the top, the electric field is applied from right to left, and the stress is tensile and applied uniaxially along x. The snapshots shown correspond to (a) $t = 0$, 1.00, 1.54, 1.76, 1.93, 2.06, 2.17, 2.34, and 2.40×10^{-2} τ, (b) $t = 0$, 0.05, 0.16, 0.47, 0.77, 1.05, 1.51, 1.94, 2.36, 2.78, 3.23, 3.70, 4.17, 4.67, 5.20, 5.76, 6.37, 7.00, 7.64, 8.27, 8.90, 9.53, 10.1, 11.2, 12.2, 14.3, and 18.5×10^{-1} τ, (c) $t = 0$, 0.06, 0.10, 0.15, 0.21, 0.27, 0.38, 0.66, 0.76, 0.81, 0.85, 0.89, 0.97, 1.08, 1.28, 1.56, and 1.90 τ; and (d) $t = 0$, 0.79, 1.63, 2.14, 3.16, 4.43, 5.89, 10.8, 17.7, 21.7, 23.5, and 25.3 τ. (e) Evolution of the perturbation amplitude, $\tilde{\Delta}$, for cases (b),(c), and an additional case with $\Xi = 1.0$ for $\tilde{k} = 0.65$ and $\tilde{\Delta}_0/\tilde{\lambda} = 0.05$. (f) Evolution of $\tilde{\Delta}$ for case (d). In (e) and (f), solid lines represent the simulation results according to the fully nonlinear model, while the data points [open circles in (e) and star symbols in (e) and (f)] correspond to the LST results for the same parameter sets and initial surface morphologies.

the current is turned back on and stabilizes the planar morphology. This stable morphological response is demonstrated further in Fig. 2(e) that depicts the evolution of the amplitude, $\tilde{\Delta}$, of the surface morphology, $\tilde{h}(\tilde{x}, \tilde{t})$; $\tilde{\Delta}(t)$ decays to zero when the (sufficiently strong) electric current is turned on, which confirms the stability (under the prescribed conditions) of the planar surface morphology. On the other hand, $\tilde{\Delta}(t)$ grows in the absence of the simultaneous action of a sufficiently strong electric field. In Fig. 2(e), the data points correspond to the LST predictions for consistent parameter sets and initial surface morphologies with those of the corresponding simulation results (solid lines). Comparing theory and simulation shows close agreement for stable surface morphological response; for unstable response, the growth rate of the resulting groove is exponential initially (i.e., in agreement with the LST predictions) but becomes faster-than-exponential eventually.

Our numerical simulations have spanned the range of conditions and wavelengths of Fig. 1 and confirmed the key findings of the LST. The LST predictions are less reliable over the "intermediate" Ξ range where $\omega(\tilde{k})$ exhibits the two maxima. Even in this region, however, the theoretical predictions, Eqs. (5) and (6), provide useful insights for understanding surface morphological evolution. For example, according to our simulations for such values of Ξ, long-wavelength perturbations [see, e.g., the $\omega(\tilde{k} \to 0) < 0$ region for $\Xi = 0.16$ in Fig. 1] decay initially and the ATG instability is apparently inhibited. This is depicted clearly in Fig. 2(d) at $\Xi = 0.16$. Nevertheless, before the perturbation decays fully, the surface undergoes a tip-splitting instability. This generates a morphology characterized by $\lambda < \lambda_c$, where λ_c corresponds to the first critical wave number $\tilde{k}_c > 0$, where ω crosses 0; subsequently, these surface features evolve toward surface cracking. The $\tilde{\Delta}(t)$ evolution in the case of Fig. 2(d) is shown in Fig. 2(f), where the simulation result (solid line) also is compared with the LST prediction (data points). The perturbation amplitude decays initially in agreement with the LST; eventually, however, $\tilde{\Delta}(t)$ stops decaying and starts growing in a manner similar to the unstable case shown in Fig. 2(e). Therefore, the LST predictions cease to be reliable beyond tip-splitting initiation.

In summary, we analyzed the morphological stability of solid surfaces under the combined action of an electric field and mechanical stress. We found that surface EM through the action of a sufficiently strong electric field can be utilized to inhibit the stress-induced ATG instability and prevent the surface cracking of stressed solids. This finding has direct implications for the prevention or healing of cracks in electrically conducting or semiconducting solids under conditions that render their response to stress elastic; the analysis, however, can be extended to account for plasticity. Our conclusions can be tested through carefully designed experimental protocols. In conjunction with previous findings [10,15,17], our study implies that proper simultaneous action of electrical and mechanical applied forces can be used to prevent mechanically-induced and/or current-induced morphological instabilities in crystalline conductors. Analogous surface morphological stability analyses can be conducted over a broad class of materials, such as magnetic and optical materials, under various external fields, leading to more general conclusions regarding the stabilization of materials morphology and/or structure by simultaneous application of multiple external forces.

Fruitful discussions with Professors I. G. Kevrekidis, P. G. Kevrekidis, F. Milstein, and S. T. Pantelides are gratefully acknowledged. This work was supported by the National Science Foundation through Grants No. CMS-0201319, CMS-0302226, and CTS-0417770 and by the Office of Basic Energy Sciences, U. S. Department of Energy through Grant No. DE-FG02-07ER46407.

*Corresponding author.
maroudas@ecs.umass.edu

[1] R. C. Hayward, D. A. Saville, and I. A. Aksay, Nature (London) **404**, 56 (2000).
[2] A. G. Boudouvis *et al.*, J. Magn. Magn. Mater. **65**, 307 (1987).
[3] R. J. Asaro and W. A. Tiller, Metall. Trans. **3**, 1789 (1972).
[4] M. A. Grinfeld, Sov. Phys. Dokl. **31**, 831 (1986).
[5] D. J. Srolovitz, Acta Metall. **37**, 621 (1989).
[6] W. H. Yang and D. J. Srolovitz, Phys. Rev. Lett. **71**, 1593 (1993).
[7] J. Berrehar *et al.*, Phys. Rev. B **46**, 13 487 (1992).
[8] L. Xia *et al.*, J. Mech. Phys. Solids **45**, 1473 (1997).
[9] M. R. Gungor, D. Maroudas, and L. J. Gray, Appl. Phys. Lett. **73**, 3848 (1998); M. R. Gungor and D. Maroudas, Surf. Sci. **432**, L604 (1999).
[10] M. R. Gungor and D. Maroudas, Int. J. Fract. **109**, 47 (2001).
[11] M. Schimschak and J. Krug, Phys. Rev. Lett. **78**, 278 (1997).
[12] R. M. Bradley, Phys. Rev. E **65**, 036603 (2002).
[13] P. Kuhn *et al.*, Phys. Rev. Lett. **94**, 166105 (2005).
[14] D. Maroudas, Appl. Phys. Lett. **67**, 798 (1995).
[15] M. R. Gungor and D. Maroudas, J. Appl. Phys. **85**, 2233 (1999); Surf. Sci. **461**, L550 (2000); J. S. Cho, M. R. Gungor, and D. Maroudas, Surf. Sci. **575**, L41 (2005); Appl. Phys. Lett. **86**, 241905 (2005); Appl. Phys. Lett. **88**, 221905 (2006); J. Appl. Phys. **101**, 023518 (2007).
[16] L. J. Gray, D. Maroudas, and M. N. Enmark, Comput. Mech. **22**, 187 (1998).
[17] M. R. Gungor and D. Maroudas, J. Appl. Phys. **101**, 063513 (2007).